Received: Added at production | Revised: Added at production | Accepted: Added at production
DOI: xxx/xxxx

ARTICLE

Experimental study of the transfer length of pre-tensioned CFRP strands using distributed fiber optic sensors

María Serrano-Mesa*[1] | Paul Merz[2] | Alex Hückler[3] | Mike Schlaich[1]

[1]Institute of Civil Engineering, TU Berlin, Gustav-Meyer-Allee 25, 13355 Berlin, Germany
[2]Dept. of Civil, Environmental and Geomatic Engineering, ETH Zurich, Stefano-Franscini-Platz 5, 8093 Zurich, Switzerland
[3]Department of Civil Engineering and Geoinformation, BHT Berlin, Luxemburger Str. 9, 13353 Berlin, Germany

Correspondence
*María Serrano-Mesa Email: m.serranomesa@tu-berlin.de

Summary

Carbon fiber reinforced polymer strands offer a corrosion-resistant alternative to steel prestressing, but their short transfer lengths increase susceptibility to splitting cracking and challenge conventional pointwise measurements. Once splitting occurs during prestress release, these methods cannot determine a valid transfer length. This study develops an experimental framework for pre-tensioned beams based on distributed fiber optic sensor data and a semi-automated evaluation method. The method determines transfer length from unsmoothed strain profiles without manual plateau selection and remains applicable to cracked specimens by identifying the last valid pre-cracking profile. It was calibrated using small-scale tests, compared with manually determined values, and benchmarked against conventional evaluation methods. Within the investigated configurations, higher concrete strength and lower prestress led to shorter transfer lengths. The ACI model agreed with measurements within 10 %, whereas other provisions overestimated transfer length by factors of 1.5–3.2, potentially underestimating the risk of end-region cracking.

KEYWORDS:
Transfer length, Bond, CFRP tendons, Prestressed concrete, Experimental testing, Distributed Fiber Optic Sensors (DFOS), Semi-automated algorithm

1 | INTRODUCTION

Carbon fiber reinforced polymers (CFRP) offer high tensile strength and corrosion resistance, enabling durable and material-efficient prestressed concrete members with reduced concrete cover[1–5]. In pre-tensioned applications, prestressing also allows the high tensile capacity of CFRP to be used effectively while improving serviceability by limiting cracking and deformation. To transfer the prestress force from the CFRP tendons to concrete in such slender components, a thorough understanding of the bond behavior is crucial[6].

The transfer length, defined as the distance over which the prestress force is transferred to the surrounding concrete, is typically shorter for CFRP than for steel[7, 8], which demands higher measurement precision. Because the prestress force is introduced over a shorter length, the bond stresses are higher and so is the risk of splitting cracking, which has led to recommended concrete covers that exceed those for steel[9, 10]. Moreover, once splitting occurs, the prestress transfer is interrupted and the transfer length can no longer be determined from the subsequent strain profiles. Recent investigations have primarily focused on recalibrating existing theoretical models using experimental data from multiple research studies and statistical analysis[9, 11]. However, the diversity in test guidelines, methods, and instrumentation technologies across the available studies poses a significant challenge, making direct comparisons of results problematic. In addition, many commonly used measurement techniques do not provide the spatial resolution needed to capture the strain development accurately enough to determine the transfer length reliably.

To address these limitations, this study employs Distributed Fiber Optic Sensors (DFOS) to measure longitudinal concrete strains in pre-tensioned concrete beams with CFRP strands. Figure 1 presents the data recorded during the prestress transfer in a 1-m beam, illustrating the evolution of concrete strain (ε_c) along the beam length (z) and over time (t). For clarity, the displayed surface uses a lower sampling frequency, whereas the blue line represents the high-temporal-resolution measurements. DFOS data were recorded at 0.2 s intervals with a spatial sampling interval of approximately 1.3 mm, corresponding to approximately 230,000 strain values per minute per meter.

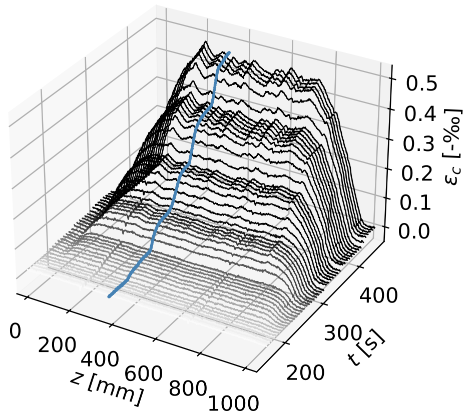

Figure 1 Concrete strain (ε_c) over time (t) and beam length (z) measured by DFOS during prestress transfer (black lines: plotted at 6-s intervals for clarity; blue line: full temporal resolution of 0.2 s).

The size and complexity of the DFOS datasets motivated a semi-automated evaluation procedure, termed the Range of Maximum Strain (RMS) method, which determines transfer length directly from unsmoothed strain profiles and thereby reduces analyst-dependent decisions. Because the measurements are quasi-continuous in time, the last pre-cracking strain profile can be identified and evaluated in specimens that crack before the prestress is fully transferred – a case that conventional end-slip and concrete-strain monitoring cannot resolve. The experimental program examines tendon diameter, prestress level and concrete strength, together with configurations of differing splitting susceptibility (concrete cover and tendon spacing). The evaluation algorithm and representative datasets are made openly available[1].

2 | BACKGROUND AND STATE OF THE ART

The bond behavior of tendons in concrete is governed by several interacting parameters, including tendon type and surface characteristics, concrete strength at release, prestress level, concrete cover, tendon spacing and arrangement, cross-sectional geometry, and release method[9]. The values and combinations of these parameters vary substantially among experimental studies, which complicates the direct comparison of the reported transfer lengths. Existing prediction models and code provisions, however, generally account for only a subset of these influences.

2.1 | Experimental frameworks for determining transfer length

Several experimental methods have been developed to investigate prestress transfer, including pull-out tests[7, 9, 12–15], the *ECADA* test[16, 17], and small-scale beam tests. A detailed description of the existing testing setups is given by Geßner[18]. While pull-out tests cannot directly determine transfer length and the *ECADA* method requires iterative specimen lengths, small-scale beam tests provide a direct assessment and are therefore adopted in this study.

[1] https://github.com/mserranomesa7/tlc-dfos

Two testing frameworks are commonly referenced: the procedures of Russell and Burns (95%AMS)[19–21] and the German DIBt guideline[13]. Whereas Russell's framework primarily specifies the evaluation procedure, the DIBt guideline additionally defines specimen geometry, tendon arrangement, and release procedures to improve repeatability.

Both guideline frameworks recommend monitoring concrete strains before and after prestress release and measuring tendon end-slip to detect possible splitting cracks. Traditionally, concrete strains have been measured using DEMEC gauges[6, 15, 22–26], electrical resistance strain gauges[27–29], or Whittemore gauges[26]. However, these methods provide measurements only at discrete locations, typically at intervals of approximately 50 mm[6, 9, 15]. This spatial resolution is insufficient for accurately characterizing CFRP tendons, for which transfer lengths as short as 140 mm have been reported[6]. To determine the transfer length, these methods evaluate the longitudinal strain profile over one half of the beam. To illustrate the differences between these approaches, the experimental data of von der Heid[15] are re-analyzed, and the resulting transfer lengths are compared in Figure 2.

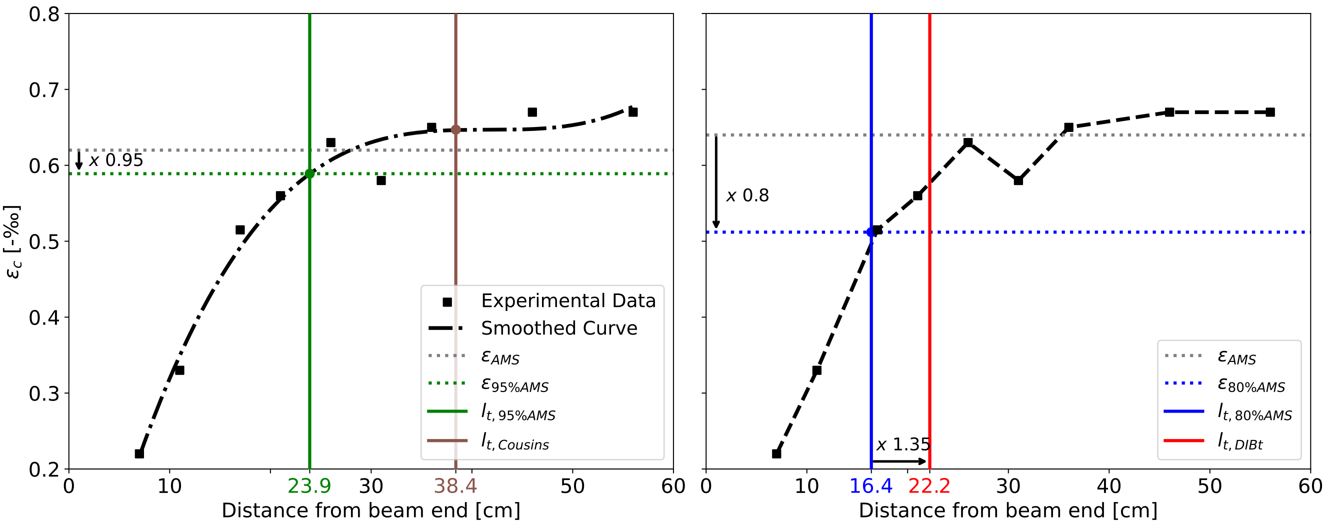

(a) 95%AMS[19–21] and Cousins[30].

(b) DIBt guideline[13].

Figure 2 Transfer length (l_t) determined from strain profiles (ε_c) over half the beam length using different evaluation methods, based on experimental data from[15].

The concrete strain is approximately zero at the beam end, increases steeply within the transfer zone, and approaches a plateau once the prestress is fully transferred. The method of Cousins *et al.*[30], based on Guyon's bond theory, defines the transfer length as the position where a smoothed strain curve levels off. The related 95%AMS method[19–21] defines it as the intersection between the smoothed strain profile and 95 % of the average maximum strain (AMS), calculated from manually selected plateau values. The DIBt guideline[13] also uses the AMS but does not require curve smoothing. It identifies the first position at which the measured strain exceeds 80 % of the AMS, denoted $l_{t,80\%\text{AMS}}$, and multiplies this distance by 1.35, a factor originally derived for steel tendons.

The reanalysis of Heid's data shows a 33 % difference between the DIBt and 95%AMS results and a deviation of up to 72 % relative to the Cousins method. These differences reflect the effects of curve smoothing, manual plateau selection, and method-specific empirical assumptions. Moreover, because these procedures were developed primarily for steel tendons, their direct applicability to CFRP tendons remains uncertain.

The high-resolution DFOS measurements used in this study address these limitations by providing dense strain profiles along the entire beam and reducing dependence on manually selected measurement points.

2.2 | Experimental investigations on transfer length of CFRP strands

Extensive research has examined the transfer length of CFRP strands and the parameters influencing it[6, 7, 15, 22–29, 31–34]. A comprehensive statistical review is provided by Jokūbaitis *et al.*[11].

Higher concrete strength at prestress release generally leads to shorter transfer lengths[22–25, 35]. The influence of prestress level is less clear: some studies report notable reductions in transfer length at high prestress levels[24, 25], while others observe a minimal effect[22, 23]. Tendon diameter, surface geometry, and roughness also significantly affect bond conditions and transfer length[7, 24]. A lower modulus of elasticity can increase bond strength through lateral expansion[26, 36]. Live ends typically show longer transfer lengths due to cutting and casting effects[27, 28].

Kueres[9] and Jokūbaitis *et al.*[11] identified concrete strength, prestress level, tendon diameter, and release method as key factors. Despite considering these parameters, the coefficient of variation between model predictions and experiments remained above 25 %[11]. Overall, contrasting results highlight the need to critically assess the theoretical models.

2.3 | Prediction models and code provisions

Several empirical and semi-empirical models have been proposed to predict the transfer length of CFRP strands, some of which have been incorporated into national guidelines. The JSCE provision[37], based on[26], adopts a simple diameter-based relationship:

$$l_t = \alpha_d \cdot d_p \tag{1}$$

where $\alpha_d = 65$ and d_p is the tendon diameter in mm.

The formulation proposed by Mahmoud *et al.*[24, 25], which forms the basis of the ACI[36] and CSA[10] provisions, additionally accounts for the prestress level and the concrete strength:

$$l_t = \frac{f_{pi} \cdot d_p}{\alpha_t \cdot f_c^{2/3}} \tag{2}$$

where f_{pi} is the initial tendon stress, f_c the concrete compressive strength at transfer, and $\alpha_t = 4.8$ for ACI and $\alpha_t = 4.4$ for CSA. The CSA provision additionally imposes a lower bound of $l_t \geq 26 \cdot d_p$.

Kueres[9] adapted the Eurocode 2[38] formulation for steel tendons by introducing coefficients for the release method, tendon type and bond conditions:

$$l_t = \frac{\alpha_1 \cdot \alpha_{2,d} \cdot f_{pi} \cdot d_p}{\eta_1 \cdot \sqrt{f_{ck}}} \tag{3}$$

where f_{ck} is the characteristic concrete compressive strength at release, $\alpha_1 = 1.0$ for gradual release, $\alpha_{2,d} = 0.34$ for CFRP strands, and $\eta_1 = 1.0$ for good bond conditions.

Figure 3 illustrates the substantial variation among selected prediction models. For typical CFRP tendons, predicted transfer lengths differ by more than a factor of three, although the underlying models were derived from similar experimental databases. Despite considerable research progress, reliable prediction of transfer length in pre-tensioned CFRP tendons therefore remains an open challenge. To address this knowledge gap, this paper presents an experimental investigation with a particular focus on developing a DFOS-based testing and evaluation framework.

3 | EXPERIMENTAL PROGRAM

3.1 | Materials

The specimens were produced using concrete of strength class C50/60 according to DIN EN 206-1[39]. The mean cube compressive strength at prestress release ranged from $f_{cm,\text{cube}} = 40$ to 70 MPa. At 28 days, the concrete reached mean cube and cylinder compressive strengths of 82.2 and 67.4 MPa, respectively. The measured tensile strength was 3.8 MPa, and the elastic modulus was 37.8 GPa.

The concrete composition per cubic meter comprised 370 kg CEM I 52.5 R cement, 156 kg water, 736 kg sand 0/2 mm, 532 kg gravel 2/8 mm, 590 kg gravel 8/16 mm, 25 kg stone-powder filler, and 3.7 kg Glenium ACE 420 superplasticizer.

Seven-wire CFRP prestressing strands manufactured by Tokyo Rope (CFCC – Carbon Fiber Composite Cable) were used[40]. Two nominal diameters, $d_p = 10.8$ and 12.5 mm, were investigated. Their nominal cross-sectional areas were $A_p = 71.3$ and 95.4 mm^2, respectively. Both strand sizes had a Young's modulus of $E_p = 126{,}000$ MPa and a tensile strength of $f_{pu} = 2137$ MPa.

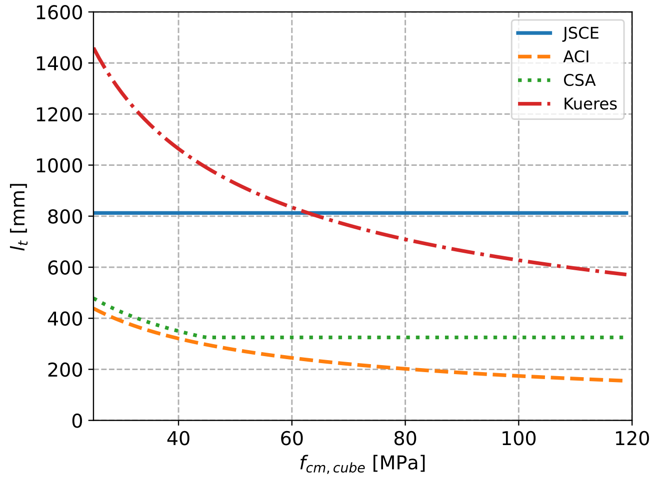

Figure 3 Transfer length (l_t) of one CFRP strand, with tendon diameter d_p = 12.5 mm and prestress level f_{pi}/f_{pu} = 60%, as a function of concrete compressive strength $f_{cm,\text{cube}}$ at prestress transfer, compared with selected models and code provisions.

3.2 | Test setup, instrumentation, and procedure

The tests were conducted according to the DIBt guideline[13], incorporating the modifications adopted in previous investigations[6, 8, 9, 15]. These modifications enable a resource-efficient investigation while limiting secondary effects associated with tendon eccentricity and cross-sectional geometry. Two horizontally arranged CFRP strands were placed symmetrically within the cross-section and prestressed in a prestressing bed, as shown in Figure 4. Because CFRP tendons are sensitive to transverse pressure, dedicated couplers supplied by *Tokyo Rope Mfg. Co. Ltd.* were used in combination with steel strands outside the specimens.

After casting, the specimens were covered with plastic film. Approximately 1–2 h before the target cube compressive strength $f_{cm,\text{cube}}$ was reached, the film and side formwork were removed and the measurement equipment was installed. Glued-on DFOS were attached to the two narrow longitudinal faces at tendon level using a fast-curing methyl-methacrylate adhesive. These two sensor lines defined measurement channels 1 and 2. Embedded DFOS were installed before casting.

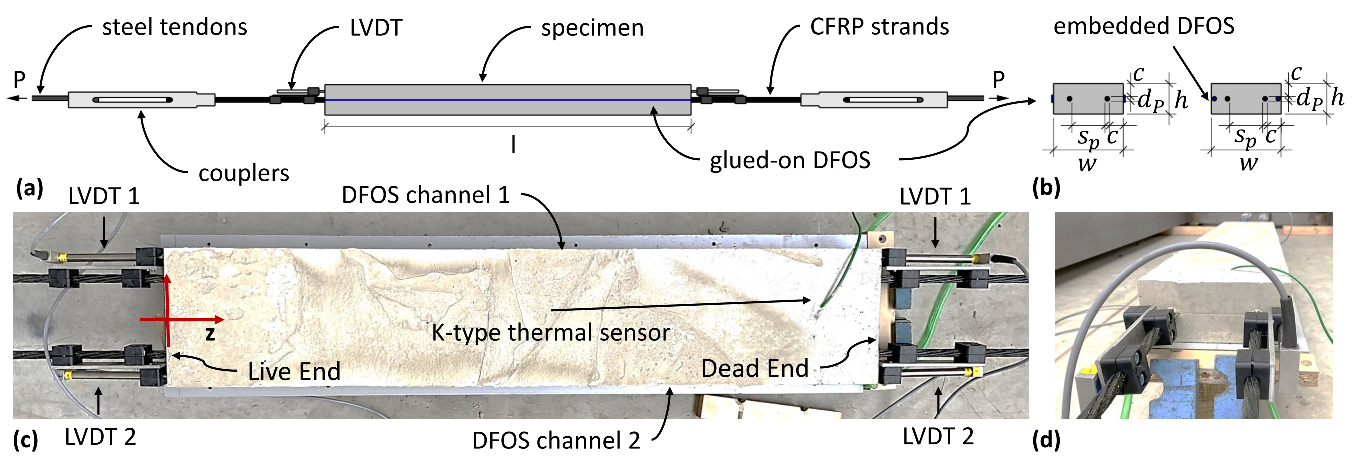

Figure 4 Test setup of the beam experiments: (a) Side view and (b) cross-sections (schematics); (c) Top view and (d) perspective view (photographs). Here, P denotes the prestressing force, l the specimen length, c the concrete cover, s_p the tendon spacing, d_p the tendon diameter, and w and h the cross-section width and height.

Two types of DFOS were used. The first, denoted *g* (glued-on), was a polyimide-coated optical fiber with an outer diameter of 155 μm. Although its alkaline resistance is limited, it is suitable for measurements in young concrete. The second, denoted *e* (embedded), was a monolithic composite sensor supplied by *Nerve-Sensors*[41]. It consisted of polyester and epoxy, had a textured surface, and had an outer diameter of approximately 3 mm.

Concrete strain was measured on both longitudinal sides of the specimens at tendon level. The embedded sensors were positioned 5 mm from the lateral surfaces to reduce the influence of internal, non-critical splitting cracks on the measurements. Specimen temperature was monitored using K-type thermal sensors to compensate for thermal effects in the DFOS data and to estimate the time at which the target concrete strength was reached according to the maturity method of De Vree[42, 43]. In four tests, linear variable displacement transducers (LVDTs) were additionally used to measure tendon end slip at both ends of the specimens. DFOS data were recorded using an ODiSI 6000 series Rayleigh-backscatter interrogator from LUNA.

After installation of the measurement equipment, the prestressing force in both tendons was transferred simultaneously to the specimen by gradually releasing the hydraulic jacks. Following the procedure used in previous investigations[8, 9, 15, 34], the prestress was released in increments of 10–20 % of the total prestressing force. The release was paused for approximately 10–20 s after each increment to inspect the transfer zones for visible splitting cracks.

3.3 Test program

The test program was designed to investigate the main parameters affecting the transfer length: tendon diameter (Test DP), concrete strength at prestress release (Tests FC), and prestressing level (Tests FP). Test DF served as the default configuration, and each parameter was varied individually, with the goal of isolating its effect. In addition, the geometric parameters of concrete cover and tendon spacing were varied in Tests -CC and FP-SP, respectively. These tests were intended to evaluate the ability of DFOS to determine the transfer length even in specimens exhibiting splitting cracks, as both parameters influence splitting behavior[10, 37]. The selected values followed existing recommendations[9, 34]. Where the cross-sectional geometry was varied, the dimensions were adjusted to maintain approximately the same concrete compressive stress due to prestressing. For the Tests -CC and based on previous findings indicating a limited influence of tendon spacing relative to concrete cover[9, 34], the spacing was adjusted to obtain the required cross-sectional area while maintaining the target cover-to-diameter ratio. All the test specimens had a length $l = 1$ m. The complete test program and the resulting transfer lengths are summarized in Table 1.

Table 1 Test program and transfer-length results. Bold values indicate the parameters varied relative to the DF configuration.

Type	d_p [mm]	$f_{cm,\text{cube}}$ [MPa]	f_{pi}/f_{pu}^{tar} [%]	c/d_p [-]	s_p/d_p [-]	$w \times h$ [mm]	Sensor(s)	Cracked	$f_{p,cr}$ [MPa]	l_t (mean/SD) [mm]
DF	12.5	42	60	2.8	7.6	190×82.5	g+LVDT	Yes	918	190/11
DP	**10.8**	40	60	2.6	6.6	146×66.0	e	Yes	963	218/14
FC	12.5	**60**	60	2.8	7.6	190×82.5	e	Yes	965	208/24
FP	12.5	44	**40**	2.8	7.6	190×82.5	g+LVDT	No	–	168/24
FP-SP	12.5	43	**40**	2.8	**2.6**	127×82.5	e	Yes	804	237/18
CC	12.5	43	60	**3.2**	5.3	171×92.5	g+LVDT	Yes	1249	351/45
CC-2	12.5	38	60	**3.2**	5.3	171×92.5	e	No	–	364/16
FC-CC	12.5	**70**	60	**3.2**	5.3	171×92.5	e	Yes	*	278/22
FC-CC-2	12.5	**68**	60	**3.2**	5.3	171×92.5	e	Yes	1199	266/35
FP-CC	12.5	43	**40**	**3.2**	5.3	171×92.5	g+LVDT	No	–	196/14

Notes: d_p: tendon diameter; $f_{cm,\text{cube}}$: cube compressive strength at release; f_{pi}/f_{pu}^{tar}: target initial prestress level; c: concrete cover; s_p: tendon spacing; $w \times h$: width×height of the cross-section; g: glued-on DFOS; e: embedded DFOS; LVDT: linear variable displacement transducer; Cracked: superficial splitting cracks during prestress transfer; $f_{p,cr}$: maximum tendon stress before cracking; l_t: transfer length (mean/standard deviation). *: no time-resolved data available. Bold: parameter varied relative to DF.

Tests CC and FC-CC were each repeated once. Test CC was repeated using the alternative sensor type. Test FC-CC was repeated because the first test provided only individual strain profiles immediately before and after critical cracking rather than continuous time-resolved measurements. The available pre-cracking profile could nevertheless be used to determine transfer length. The duplicate tests are denoted CC-2 and FC-CC-2. All other parameter combinations were represented by a single specimen, yielding four transfer-length evaluations from two measurement channels at both beam ends. The limited number of repeated specimens should therefore be considered when interpreting the observed parameter effects. Nevertheless, the controlled test conditions and high-resolution DFOS measurements enabled detailed comparison of the investigated configurations.

4 | DFOS DATA PROCESSING AND TRANSFER-LENGTH EVALUATION

4.1 | Pre-processing: Identification of the critical prestress level

Transfer length can only be determined from strain profiles recorded before critical splitting cracking alters the prestress-transfer mechanism. Conventionally, the onset of critical cracking is identified during prestress release by monitoring tendon end slip using linear variable displacement transducers (LVDTs). Figure 5 compares the measured end slip for a crack-free specimen and a specimen that developed superficial splitting cracks.

The normalized introduced prestress is expressed as P_i/P_{tot}, where P_i is the prestressing force introduced to the specimen at a given stage and P_{tot} is the total prestressing force before release. LVDT 1 and LVDT 2 correspond to the two specimen sides and are aligned with DFOS measurement channels 1 and 2, respectively, as shown in Figure 4.

In the crack-free Test FP, the tendon slip s increased gradually during prestress release and showed a small additional increase during the pauses between release steps due to time-dependent bond slip. The final slip remained below 0.9 mm, as shown in Figure 5a. In Test CC, by contrast, a pronounced increase in slip occurred during the final release stage and was accompanied by superficial splitting cracking, resulting in slip values exceeding 2 mm (Figure 5b). The reliability of the LVDT measurements was limited during the final release stages because the strands became slack outside the specimen and the weight of the couplers influenced the measured end slip. The LVDTs indicated whether critical cracking had occurred; however, they did not allow the prestress level immediately before cracking to be identified accurately.

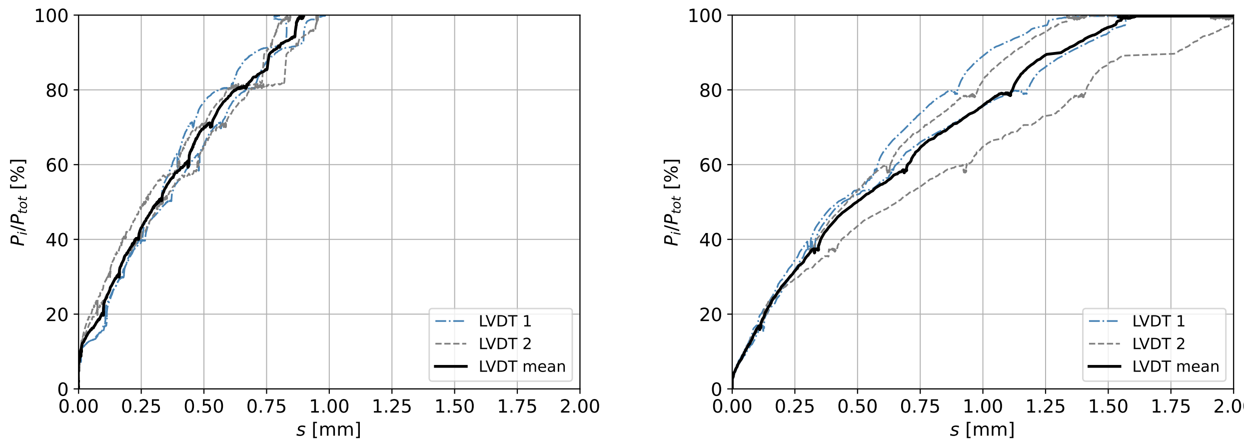

(a) **(b)**

Figure 5 Tendon slip s measured during prestress release vs. the introduced prestress force P_i/P_{tot} using LVDTs corresponding to the two DFOS measurement channels (LVDT 1 and 2); the mean curve is also shown. (a) Crack-free Test FP; (b) Test CC with superficial splitting cracks.

In contrast, DFOS enable a more precise identification of the critical prestress level because they record the strain distribution over time quasi-continuously during the prestress release process, without requiring measurement stops. Figure 6a shows the concrete strain (ε_c) plotted over the beam length (z) for increasing introduced prestress (P_i/P_{tot}). As long as the prestress is effectively transferred, the strain profiles maintain a characteristic, smooth shape. When critical cracking occurs, this shape suddenly breaks down and the strain values drop, indicating a loss of prestress transfer.

However, this breakdown does not occur uniformly along the beam: at the onset of cracking, some positions exhibit an abrupt strain loss while others momentarily still show increasing strain, as force redistributes to the regions that remain bonded

(Figure 6a, near the live end). A criterion based on a single position would, therefore, misidentify the onset of cracking. To reduce this sensitivity, the detection criterion is based on the integral of each strain profile over the specimen length, computed over time (Figure 6b). The integral increases steadily as prestress transfer progresses and drops abruptly when cracking occurs. The onset of the abrupt drop defines the critical time t_{cr}. The corresponding prestress level is denoted P_{cr}/P_{tot}, and the strain profile immediately before t_{cr} is used to determine the transfer length.

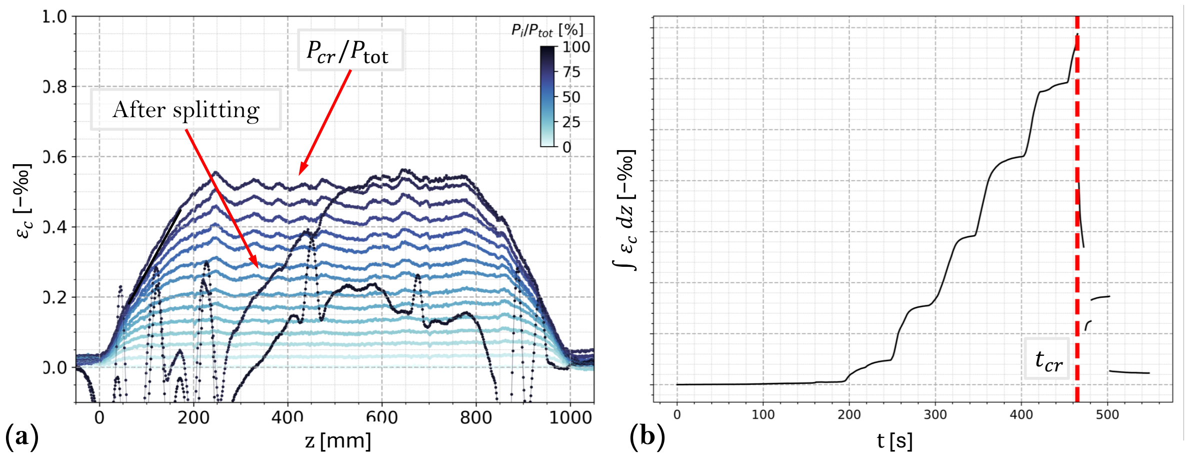

Figure 6 DFOS concrete strain measurements for Test DP, channel 2: (a) strain distributions (ε_c) along the beam at increasing introduced prestress level P_i/P_{tot}; (b) identification of the critical time t_{cr} from the strain integral ($\int \varepsilon_c\, dz$), with $P_{cr}/P_{tot} = 76\,\%$.

4.2 | Transfer length determination based on the RMS method

Conventional strain-based evaluations determine the transfer length from the AMS, which requires manual selection of the plateau region or curve smoothing, as illustrated in Figure 2, and might therefore introduce subjectivity. With the number of strain profiles recorded by DFOS, a semi-automated evaluation is preferable. Moreover, the existing formulations were originally calibrated for steel tendons and are therefore not necessarily transferable to CFRP. To address these limitations, a new Range of Maximum Strain (RMS) method was developed to determine transfer length from DFOS data with reduced analyst dependence and without curve smoothing, replacing manual plateau selection with a histogram-based procedure.

Instead of manually selecting a single AMS value, the strain histogram is analyzed to identify the interval with the highest concentration of measurements, defined as the RMS region. The histogram is constructed using fixed intervals of width $\Delta\varepsilon_c$, beginning at $\varepsilon_c = 0$. The most populated interval defines the RMS region and represents the approximately constant-strain plateau beyond the transfer zone.

The transfer length is defined as the first position from each beam end at which the measured strain enters the RMS interval. To prevent isolated measurements within the transfer zone from being identified as the beginning of the plateau, the admissible length of outliers l_{ol} defines the maximum spatial interruption permitted within an otherwise continuous sequence of values belonging to the RMS interval. The first position of the accepted plateau sequence defines the transfer length at the live end ($l_{t,le}$) or dead end ($l_{t,de}$). As illustrated in Figure 7, the embedded sensor in Test DP, channel 1, produces a smooth strain profile, whereas the glued-on sensor in Test DF, channel 1, exhibits greater point-to-point scatter. In both cases, the RMS region is identified consistently and yields plausible live- and dead-end transfer lengths.

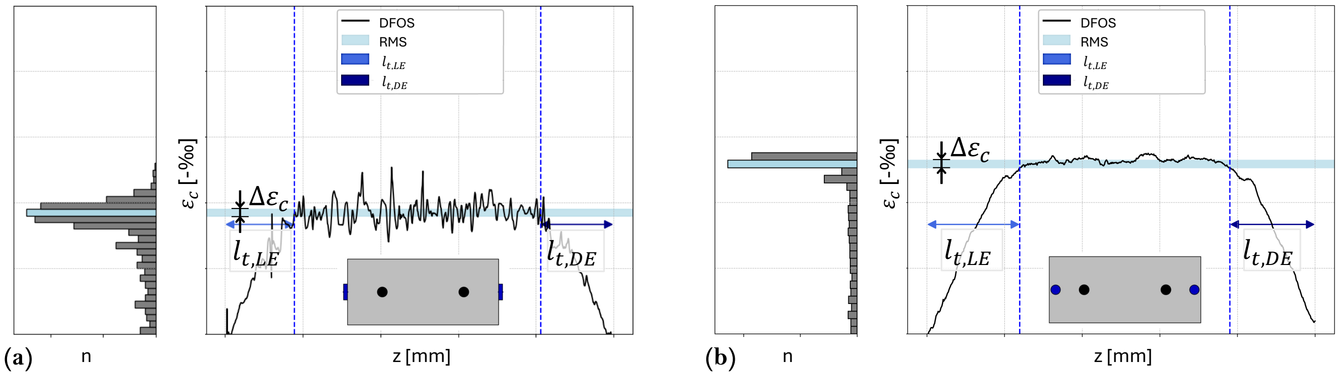

Figure 7 Transfer length determination using the RMS method: histogram-based identification of the RMS region (left) and strain distribution along the specimen (right), for (a) Test DF with glued-on DFOS and (b) Test DP with embedded DFOS.

5 | RESULTS AND DISCUSSION

5.1 | Experimental transfer-length results

Figure 8 presents the transfer lengths determined using the RMS method. For each specimen, four values were obtained from the two DFOS measurement channels and the live and dead beam ends. The individual values are shown together with their mean, which is also reported in Table 1.

The live-end transfer lengths were, on average, 4.9 % greater than the corresponding dead-end values. This difference is consistent with the asymmetric release conditions reported in previous investigations [27, 29]. The mean absolute relative difference between the two measurement channels was 0.8 %, indicating no pronounced lateral asymmetry in the measured prestress-transfer behavior.

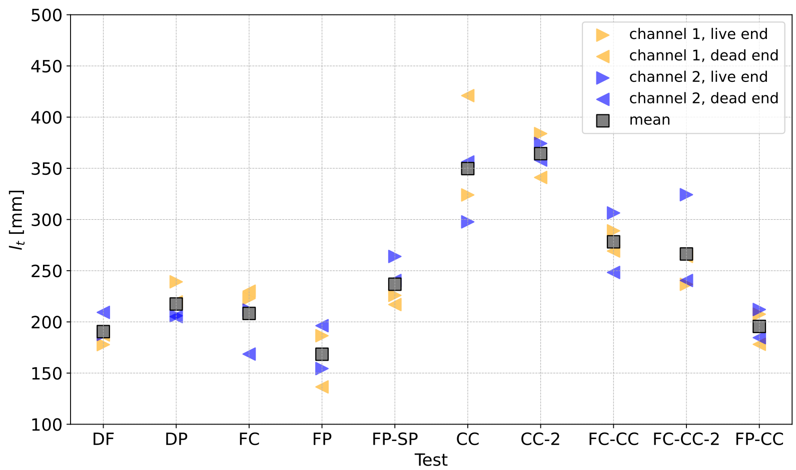

Figure 8 Transfer lengths l_t determined using the RMS method for DFOS measurement channels 1 and 2 and the live and dead beam ends. Individual values are represented by triangles pointing toward the corresponding beam end, and mean values are shown as black squares.

The K-type thermal sensors allowed for the accurate determination of the time at which the required concrete strength for prestress release was reached, with an average deviation between the achieved and the target compressive concrete strength of approximately 3 % relative to the target value. Both DFOS types proved suitable within the presented framework. The embedded sensors produced smoother strain profiles (Figure 7), whereas the glued-on sensors exhibited greater point-to-point scatter, which motivated the introduction of the admissible outlier length l_{ol}. Both were nevertheless evaluated reliably using the same parameter set: Tests CC and CC-2, which were carried out with the two sensor types, yielded mean transfer lengths within 4 % of each other despite differing concrete strengths at release. The embedded sensors were also less demanding to install, as they were placed before casting and required no surface preparation within the short interval between formwork removal and prestress release. Both types resolve the transfer zone with a spatial sampling interval more than an order of magnitude finer than the approximately 50 mm spacing of DEMEC measurements[6, 9, 15], so that the choice between them can be based on practical considerations rather than on measurement resolution.

5.2 | Calibration and evaluation of the DFOS-RMS approach

The RMS parameters $\Delta\varepsilon_c$ and l_{ol} were calibrated against manually determined reference transfer lengths, defined at the transition from the increasing-strain region to the approximately constant-strain plateau. A grid search was performed for every combination of $0.010 \leq \Delta\varepsilon_c \leq 0.030$ ‰ in increments of 0.001 ‰ and $10 \leq l_{ol} \leq 30$ mm in increments of 1 mm. For each combination, the mean absolute relative difference between the RMS-based and manually determined reference transfer lengths was calculated. The combination minimizing this difference was selected.

The optimal parameters differed only slightly between sensor types ($\Delta\varepsilon_c = 0.023$ ‰, $l_{ol} = 17$ mm for embedded and 0.020 ‰, 16 mm for glued-on, with mean absolute relative differences of 7.1 and 12.4 %). Common values of $\Delta\varepsilon_c = 0.020$ ‰ and $l_{ol} = 17$ mm were therefore adopted and applied to all specimens without sensor-specific adjustment, giving a mean absolute relative difference of 8.1 % from the manual reference values.

Figure 9 compares the RMS results with those obtained using the 95%AMS method and the DIBt guideline. The 95%AMS method showed a mean absolute relative difference of 9.6 % from the manually determined values, which was comparable to the difference obtained using RMS. The DIBt procedure showed a larger mean absolute relative difference of 12.0 %. The similar results obtained using RMS and 95%AMS may be explained by the comparable strain levels used to identify the end of the transfer zone. The RMS method defines transfer length at the first accepted position entering the RMS interval, whereas the 95%AMS method defines it at 95 % of the average plateau strain. The larger difference obtained using the DIBt procedure may partly result from its empirical factor of 1.35, which was originally established for steel prestressing tendons.

The comparison primarily assesses the consistency of the RMS method with established procedures rather than providing an independent evaluation of the 95%AMS and DIBt methods. In the present analysis, the plateau strain required by both conventional procedures was derived automatically from the center of the RMS interval, thereby removing the manual plateau selection normally involved in their application. In addition, all methods were applied to the same high-resolution DFOS data, so the comparison does not reflect the substantially lower spatial resolution of conventional DEMEC measurements. The principal advantage of RMS is therefore not a substantially closer agreement with the reference values than that achieved by 95%AMS, but its fully data-driven evaluation, which avoids manual plateau selection as well as predefined equations and empirical coefficients.

5.3 | Influence of the investigated parameters

The effect of the investigated parameters is best assessed jointly with the maximum prestress introduced before critical splitting cracks appeared ($f_{p,cr}$, Table 1), since specimens that cracked early had to be evaluated at this lower prestress level rather than at the target value. Comparing tests at equal cover, a higher concrete strength reduced the transfer length by about 21–27 % (e.g., FC-CC, FC-CC-2 vs. CC, CC-2), consistent with a more rapid prestress transfer, i.e., shorter length needed to introduce the prestress force. A larger concrete cover appeared to increase the transfer length (e.g., DF vs. CC), but this is attributable to the higher prestress level it allowed before cracking rather than to cover itself. The effect of prestress level was clearer: at equal cover, FP-CC (40 %) showed a transfer length about 45 % shorter than CC and CC-2 (60 %), since a lower prestress force requires a shorter length to be introduced. The expected reduction for the smaller tendon diameter (Test DP vs. DF) was not observed, likely offset by the higher $f_{p,cr}$; reduced tendon spacing increased the transfer length by 41 % , but it is based solely on the single FP-SP specimen and the available literature does not establish a consistent effect for comparable CFRP configurations.

Splitting cracking was observed across most configurations. Increasing the cover-to-diameter ratio from 2.8 to 3.2 raised the prestress force introduced before splitting but did not reliably prevent it, whereas at normal tendon spacing the specimens prestressed to 40 % remained crack-free, even at $c/d_p = 2.8$. Since seven of the ten specimens cracked before prestress release was completed, most of the investigated parameter combinations became accessible only through the pre-cracking evaluation enabled by the DFOS-RMS approach.

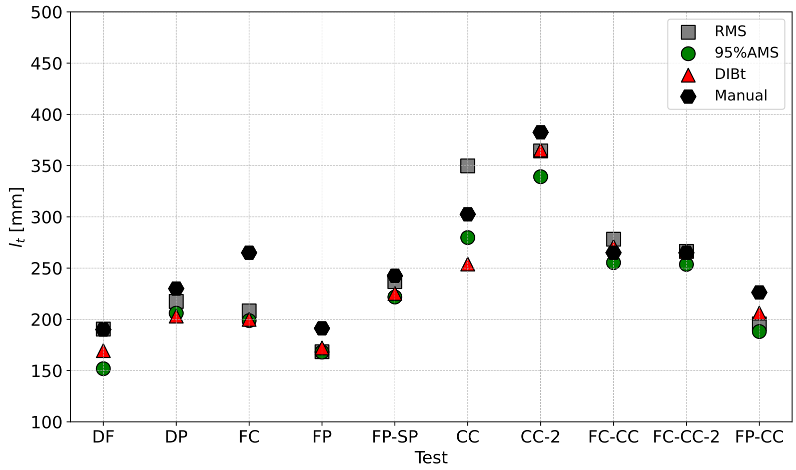

Figure 9 Transfer lengths determined using the RMS method, the 95%AMS method, and the DIBt guideline, compared with the manually determined reference values.

5.4 | Comparison with prediction models and code provisions

The comparison of the experimental transfer lengths with the summarized prediction models and code provisions is shown in Figure 10. In Eqs. (2) and (3), f_{pi} was taken for cracked specimens as $f_{p,cr}$, i.e., the tendon stress at the instant at which the experimental transfer length was determined, so that predictions and measurements refer to the same state of prestress transfer. For Test FC-CC, no time-resolved data were available. However, critical cracking occurred analogously to Test FC-CC-2, approximately one minute after the completion of prestress release. Therefore, the tendon stress at cracking was assumed to correspond to the target prestress level for this test. The experimentally measured cube compressive strengths were converted to the corresponding concrete strength values required in the prediction equations according to[44].

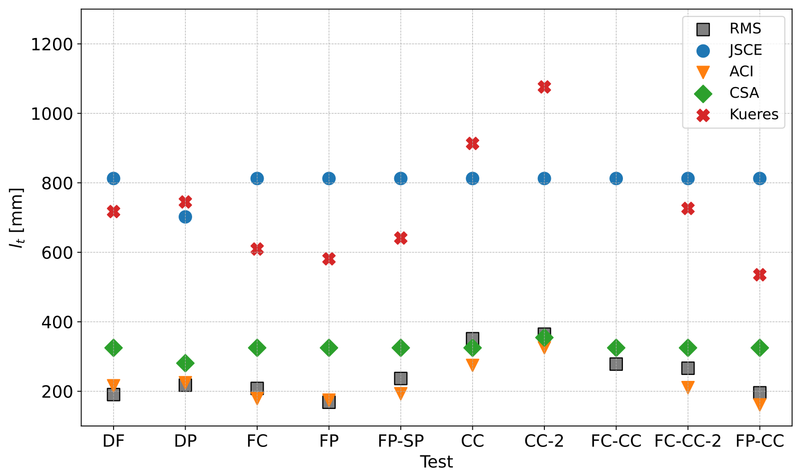

Figure 10 Experimental transfer lengths l_t determined using the RMS method compared with selected prediction models and code provisions in Eqs. (1)–(3).

The JSCE model[37], which is based solely on tendon diameter, produced the largest predicted values. Depending on the configuration, the predictions were approximately 2.4–3.2 times the measured transfer lengths. The formulation proposed by Kueres[9], which adapts the Eurocode 2 approach for steel prestressing tendons, also overestimated the experimental results by approximately a factor of two.

The CSA model[10] provided closer estimates but still overestimated the measured values by approximately 50 % on average. This difference was influenced by the prescribed lower bound of $l_t \geq 26d_p$.

The overestimation of transfer length is not necessarily conservative for all design considerations. If the actual transfer length is shorter than assumed, the prestress force develops more rapidly near the member end. This may increase local tensile stresses and the risk of early-age end-region cracking. Consequently, an overestimated transfer length may conceal critical serviceability behavior.

The closest agreement was obtained using the formulation proposed by the ACI model[36]. Its predictions differed from the experimental results by approximately 10 % on average. This agreement is not surprising, as the formulation was calibrated using the same CFRP strands, comparable geometries, and parameter ranges that largely cover the values investigated here (e.g.,[22–25, 31]). By contrast, the broader compilation by Jokūbaitis *et al.*[11] reports mean deviations exceeding 25 % for a wider range of geometries, CFRP tendon types, and tendon layouts.

5.5 | Limitations and outlook

Additional systematic studies are needed to expand the investigated parameter space. On the tendon side, the influence of tendon type, surface geometry and Young's modulus should be examined for different CFRP products. On the concrete side, broader ranges of concrete strength and elastic modulus, alternative section geometries, and multi-strand configurations should be evaluated, given their potential effects on transfer length.

Approval-oriented test campaigns for CFRP tendons should include larger specimen numbers and, for cases with longer transfer lengths (e.g., Test CC-2), longer beams to provide a sufficiently broad plateau region of at least 50 cm. Improved installation techniques for glued DFOS may help reduce local outliers. The framework could also be extended to tendons with integrated or embedded DFOS, provided the sensor can be installed during tendon manufacture, to enable direct measurement of tendon strains. Because tendon strains are substantially higher than concrete strains, this application may require adjustment of the parameter $\Delta\varepsilon_c$. The developed DFOS-RMS framework provides a solid basis for future investigations of prestress transfer in CFRP tendons.

6 | CONCLUSIONS

This study developed and validated a DFOS-based framework for determining the transfer length of pre-tensioned CFRP strands, including specimens that developed splitting cracks during prestress release. The main conclusions are:

- Conventional experimental frameworks based on end-slip and discrete concrete-strain measurements, such as LVDTs and DEMEC gauges, may detect splitting cracking but cannot identify the last valid pre-cracking strain profile with sufficient spatial and temporal resolution. The developed DFOS-RMS approach identifies the onset of cracking, extracts the last valid pre-cracking profile, and quantifies the maximum prestress reached before cracking.
- The proposed RMS algorithm determines transfer length directly from unsmoothed DFOS strain profiles using histogram analysis, without manual plateau selection. Its two parameters – the histogram interval width and admissible length of outliers – were calibrated against manually determined reference values, resulting in a mean absolute relative difference of 8.1 %, comparable to established evaluation methods.
- Both glued-on and embedded DFOS were suitable for the proposed framework. The mean absolute relative difference between the two measurement channels was 0.8 %, while live-end transfer lengths were, on average, 4.9 % greater than dead-end values.
- Within the investigated configurations, increasing concrete strength reduced transfer length by approximately 25 %, while reducing the target prestress level from 60 % to 40 % resulted in an approximately 45 % shorter transfer length at comparable cover.
- For the investigated CFCC strands and parameter range, the ACI predictions differed from the measurements by 10 % on average, whereas the other evaluated models overestimated them by factors of 1.5 to 3.2. Such overestimation is not necessarily conservative for end-region cracking and this wide range highlights the substantial inconsistency among current code provisions.

The DFOS–RMS framework enables transfer-length evaluation in specimens that crack before prestress release is completed and quantifies the maximum prestress reached before critical cracking. It provides a basis for larger, systematically replicated test programs and for improving approval procedures and prediction models for CFRP tendons. Validation across additional CFRP products, cross-sections, concrete properties, and tendon arrangements is required before general design recommendations can be established.

NOTATION

A_p	nominal cross-sectional area of a CFRP strand
c	concrete cover
d_p	nominal diameter of the CFRP strand
E_p	Young's modulus of the CFRP strand
f_c	concrete compressive strength at transfer
f_{ck}	characteristic concrete compressive strength
$f_{cm,\text{cube}}$	mean cube compressive strength
f_{pi}	initial tendon stress
$f_{p,cr}$	tendon stress at the onset of critical splitting cracking
f_{pu}	tensile strength of the CFRP strand
h	height of the cross-section
l	specimen length
l_{ol}	admissible length of outliers
l_t	transfer length
$l_{t,80\%\text{AMS}}$	distance to the first strain exceeding 80 % AMS
$l_{t,de}$	transfer length at the dead end
$l_{t,le}$	transfer length at the live end
P_{cr}	prestressing force at the onset of critical splitting cracking
P_i	prestressing force at a given release stage
P_{tot}	total prestressing force before release
s	tendon end slip
s_p	tendon spacing
t	time
t_{cr}	time at the onset of critical splitting cracking
w	width of the cross-section
z	longitudinal distance to beam live end
α_1	coefficient accounting for the release method
$\alpha_{2,d}$	coefficient accounting for the tendon type
α_d	diameter coefficient (JSCE)
α_t	bond coefficient (ACI, CSA)
$\Delta\varepsilon_c$	histogram interval width
ε_c	concrete strain
η_1	coefficient accounting for bond conditions
ACI	American Concrete Institute
AMS	average maximum strain
CFCC	carbon fiber composite cable
CFRP	carbon fiber reinforced polymer
CSA	Canadian Standards Association
DEMEC	demountable mechanical strain gauge
DFOS	distributed fiber optic sensors
DIBt	Deutsches Institut für Bautechnik
JSCE	Japan Society of Civil Engineers
LVDT	linear variable displacement transducer
RMS	range of maximum strain
SD	standard deviation

AUTHOR CONTRIBUTIONS

Conceptualization: MSM and PM; Methodology: MSM and PM; Experimental work: MSM; Software and evaluations: MSM; Writing and original draft preparation: MSM; Review and editing: MSM, PM, AH and MS; Supervision: AH and MS; Funding acquisition: AH and MS. All authors have read and agreed to the published version of the article.

ACKNOWLEDGMENTS

The authors gratefully acknowledge the contribution of Oliver Disse, who supported the development and implementation of the data-processing code through a student research project completed as part of his Master's studies. Open access funding provided by Technische Universität Berlin.

FUNDING INFORMATION

The authors gratefully acknowledge the financial support of the German Federal Ministry of Transport and the Federal Ministry of Education and Research under grant number 03ZZ0358A, as well as the support provided by Hentschke Bau GmbH.

CONFLICT OF INTEREST STATEMENT

The authors declare that they have no conflicts of interest that could have influenced the work reported in this manuscript.

DATA AVAILABILITY STATEMENT

The executable tool and a representative dataset used in this study are available as open-source materials in the following GitHub repository: https://github.com/mserranomesa7/tlc-dfos, DOI: https://doi.org/10.5281/zenodo.19450526. Due to the large size of the full dataset, it is not publicly hosted but can be obtained from the corresponding author upon reasonable request.

DECLARATION OF GENERATIVE AI AND AI-ASSISTED TECHNOLOGIES IN THE WRITING PROCESS

ChatGPT (OpenAI, GPT-5.6 Thinking; used 2026) was used for language editing, restructuring, and clarity improvements in the document. It was not used to generate data or perform the reported analyses. All outputs were reviewed and verified by the authors against the experimental results, analysis scripts, cited literature, and original manuscript. No sensitive, confidential, proprietary, or human-subject data were entered into the tool. The authors take full responsibility for the final content.

ORCID

María Serrano-Mesa https://orcid.org/0000-0001-8941-7141
Paul Merz https://orcid.org/0000-0002-2110-5456
Alex Hückler https://orcid.org/0000-0001-8675-6965
Mike Schlaich https://orcid.org/0009-0005-5728-0247

References

1. Kromoser B, Preinstorfer P, and Kollegger J. Building lightweight structures with carbon-fiber-reinforced polymer-reinforced ultra-high-performance concrete: research approach, construction materials, and conceptual design of three building components. Structural Concrete. 2019;**20**:730–744.

2. May S, Steinbock O, Michler H, and Curbach M. Precast slab structures made of carbon reinforced concrete. Structures. 2019;**18**:20–27.

3. Loufti J, Dombrowski M, Merz P, Eddin A, and Schlaich M. Interdisciplinary optimisation tool for doubly curved beam-like shell floors made of CFRP prestressed concrete. In: Proceedings of IASS Annual; 2024. Available from: https://app.iass2024.org/files/IASS_2024_Paper_405.pdf.

4. Garg N, and Shrivastava S. Environmental and economic comparison of FRP reinforcements and steel reinforcements in concrete beams based on design strength parameter. In: Proceedings of the UKIERI Concrete Congress, Jalandhar, India; 2019. p. 5–8.

5. Khorgade P, Rettinger M, Burghartz A, and Schlaich M. A comparative cradle-to-gate life cycle assessment of carbon fiber-reinforced polymer and steel-reinforced bridges. Structural Concrete. 2023;**24**(2):1737–1750.

6. Stark A, Classen M, and Hegger J. Bond behaviour of CFRP tendons in UHPFRC. Engineering Structures. 2019;**178**:148–161.

7. Stark A, and Hegger J. Verbundverhalten von CFK-Spannbewehrungen in UHPFRC. Beton-und Stahlbetonbau. 2013;**108**(10):701–710.

8. Serrano-Mesa M, Jesse F, Hückler A, and Schlaich M. Untersuchung des Verbundverhaltens von CFK-Spannlitzen in Beton mit faseroptischen Sensoren. Beton- und Stahlbetonbau. 2023;**118**(10):744–756.

9. Kueres S. Analysis and design of concrete beams with pre-tensioned reinforcement (PhD thesis). RWTH Aachen University. Aachen, Germany; 2019. Available from: https://publications.rwth-aachen.de/record/785589.

10. CSA Standard S806-12. Design and construction of building structures with fibre-reinforced polymers. Canadian Standards Association (CSA); 2012.

11. Jokūbaitis A, and Valivonis J. An analysis of the transfer lengths of different types of prestressed fiber-reinforced polymer reinforcement. Polymers. 2022;**14**(19):3931.

12. International Union of Testing and Research Laboratories for Materials and Structures (RILEM). RC 6 TC9-RC: Bond test for reinforcement steel. 2. Pull-out test; 1983.

13. Deutsches Institut für Bautechnik. DIBt: Richtlinien für die Prüfung von Spannstählen auf ihre Eignung zur Verankerung durch sofortigen Verbund. Mitteilungen IfBt, Heft 6/1980; 1980.

14. Bertram G. Zum Verbund- und Querkrafttragverhalten von Spannbetonträgern aus ultra-hochfestem Beton (PhD thesis). RWTH Aachen University. Aachen, Germany; 2012. Available from: http://publications.rwth-aachen.de/record/62521.

15. von der Heid AC. Zum Tragverhalten von Sandwichelementen aus Textilbeton mit schlaffer und vorgespannter Bewehrung (PhD thesis). RWTH Aachen University. Aachen, Germany; 2021. Available from: https://publications.rwth-aachen.de/record/818012.

16. Martí-Vargas JR, Serna-Ros P, Fernández-Prada MA, Miguel-Sosa PF, and Arbeláez CA. Test method for determination of the transmission and anchorage lengths in prestressed reinforcement. Magazine of Concrete Research. 2006;**58**(1):21–29.

17. Oller E, Ortiz G, Prazeres NV, Murcia-Delso J, and Marí A. Experimental bond performance of fibre reinforced polymer prestressed concrete elements. In: International Symposium of the International Federation for Structural Concrete. Springer; 2023. p. 1133–1142.

18. Geßner S. Bond and anchorage of pre-tensioning tendons (PhD thesis). RWTH Aachen University. Aachen, Germany; 2017. Available from: http://publications.rwth-aachen.de/record/751837/files/751837.pdf.

19. Russell BW. Design guidelines for transfer, development and debonding of large diameter seven wire strands in pretensioned concrete girders. The University of Texas at Austin; 1992.

20. Russell BW, and Burns NH. 1993. *Design guidelines for transfer, development and debonding of large diameter seven wire strands in pretensioned concrete girders*. . Austin, TX, USA: Center for Transportation Research, The University of Texas.

21. Russell BW, and Burns NH. Measurement of transfer lengths on pretensioned concrete elements. Journal of Structural Engineering. 1997;**123**(5):541–549.

22. Domenico NG. Bond properties of CFCC prestressing strands in pretensioned concrete beams (Master's thesis). University of Manitoba. Winnipeg, Canada; 1996.

23. Domenico NG, Mahmoud ZI, and Rizdalla SH. Bond properties of carbon fiber composite prestressing strands. Structural Journal. 1998;**95**(3):281–290. Available from: https://www.concrete.org/publications/internationalconcreteabstractsportal.aspx?m=details&id=546.

24. Mahmoud ZI. Bond characteristics of fibre reinforced polymers prestressing reinforcement (PhD thesis). Alexandria University. Alexandria, Egypt; 1997.

25. Mahmoud ZI, Rizkalla SH, and Zaghloul EER. Transfer and development lengths of carbon fiber reinforced polymers prestressing reinforcement. ACI Structural Journal. 1999;**96**:594–602.

26. Ehsani MR, Saadatmanesh H, and Nelson CT. Transfer and flexural bond performance of aramid and carbon FRP tendons. PCI journal. 1997;**42**(1):76–86.

27. Joshi K. Investigation of carbon fiber composite cables (CFCC) in prestressed concrete piles (PhD thesis). The Florida State University. Tallahassee, FL, USA; 2013.

28. Roddenberry M, Mtenga P, and Joshi K. 2014. *Investigation of carbon fiber composite cables (CFCC) in prestressed concrete piles*. . Tallahassee (FL): Florida Department of Transportation. Available from: https://rosap.ntl.bts.gov/view/dot/27245.

29. Rambo-Roddenberry M, Joshi K, Fallaha S, Herrera R, Kampmann R, Chipperfield J, et al. Construction, strength, and driving performance of carbon-fiber-reinforced polymer prestressed concrete piles. PCI Journal. 2016;.

30. Cousins TE, Johnston DW, and Zia P. Transfer and development length of epoxy coated and uncoated prestressing strand. PCI journal. 1990;**35**(4):92–103.

31. Grace NF. Transfer length of CFRP/CFCC strands for double-T Girders. PCI journal. 2000;**45**(5). Available from: http://worldcat.org/oclc/12789822.

32. Grace NF, Enomoto T, Sachidanandan S, and Puravankara S. Use of CFRP/CFCC reinforcement in prestressed concrete box-beam bridges. ACI Materials Journal. 2006;**103**(1):123. Available from: https://ltu.edu/wp-content/uploads/2025/04/Use-of-CFRP-CFCC-Reinforcement-in-Prestressed-Concrete_2006.pdf.

33. Grace NF, Enomoto T, Abdel-Mohti A, Tokal Y, and Puravankara S. Flexural behavior of precast concrete box beams post-tensioned with unbonded, carbon-fiber-composite cables. PCI journal. 2008;**53**(4). Available from: http://worldcat.org/oclc/12789822.

34. Stark A. Analysis of prestressed sandwich panels with ultra-high performance concrete facings (PhD thesis). RWTH Aachen University. Aachen, Germany; 2017. Available from: https://publications.rwth-aachen.de/record/699418.

35. Motwani P, and Laskar A. Finite Element Studies on Transfer Length of Fiber Reinforced Polymer Strands in Pretensioned Members. In: Proceedings of the International Conference on Composite Materials and Structures-ICCMS; 2017. p. 1–10.

36. ACI Committee 440. Prestressing concrete structures with FRP tendons. American Concrete Institute (ACI 440.4R-04); 2011.

37. JSCE Concrete Engineering Series No 23. Recommendation for design and construction of concrete structures using continuous fiber reinforcing materials. Japan Soc. of Civil Engineers (JSCE); 1997.

38. Eurocode 2: Design of Concrete Structures – Part 1-1: General Rules – Rules for Buildings, Bridges and Civil Engineering Structures. Brussels: European Committee for Standardization (CEN); 2023. EN 1992-1-1:2023.

39. European Committee for Standardization (CEN). Concrete – Specification, performance, production and conformity (EN 206:2013 + A2:2021). Brussels: CEN; 2021.

40. Tokyo Rope International INC . CFCC Data Sheet; 2024. Available from: https://tokyorope-intl.co.jp/content/pdf/acfr/CFCC_Specifications.pdf.

41. NERVE-SENSORS. Epsilon Sensor; 2024. Available from: https://www.shmsystem.pl/wp-content/uploads/2022/03/EpsilonSensor.pdf.

42. De Vree RT, and Tegelaar RA. Gewichtete Reife des Betons: kontinuierliche, zerstörungsfreie Ermittlung der Betondruckfestigkeit. Beton. 1998;p. 674.

43. Soutsos M, Kanavaris F, and Hatzitheodorou A. Critical analysis of strength estimates from maturity functions. Case Studies in Construction Materials. 2018;**9**.

44. DIN EN 1992-1-1/NA:2013-04. National Annex – Nationally Determined Parameters – Eurocode 2: Design of Concrete Structures – Part 1-1: General Rules and Rules for Buildings; German Version EN 1992-1-1/NA:2013-04. Berlin: Deutsches Institut für Normung e.V.; 2013. DIN EN 1992-1-1/NA:2013-04.

□